

REPORT

 OPEN ACCESS

Structure of the human dimeric ATM kinase

Wilson C. Y. Lau^{a,b}, Yinyin Li^c, Zhe Liu^d, Yuanzhu Gao^c, Qinfen Zhang^c, and Michael S. Y. Huen^{a,b}

^aSchool of Biomedical Sciences, The University of Hong Kong, Hong Kong; ^bState Key Laboratory of Brain and Cognitive Sciences, The University of Hong Kong, Hong Kong; ^cState Key Laboratory of Biocontrol, School of Life Sciences, Sun Yat-sen University, Guangzhou, China; ^dGuangdong Provincial Center for Disease Control and Prevention, Guangzhou, China

ABSTRACT

DNA-double strand breaks activate the serine/threonine protein kinase ataxia-telangiectasia mutated (ATM) to initiate DNA damage signal transduction. This activation process involves autophosphorylation and dissociation of inert ATM dimers into monomers that are catalytically active. Using single-particle electron microscopy (EM), we determined the structure of dimeric ATM in its resting state. The EM map could accommodate the crystal structure of the N-terminal truncated mammalian target of rapamycin (mTOR), a closely related enzyme of the phosphatidylinositol 3-kinase-related protein kinase (PIKK) family, allowing for the localization of the N- and the C-terminal regions of ATM. In the dimeric structure, the active sites are buried, restricting the access of the substrates to these sites. The unanticipated domain organization of ATM provides a basis for understanding its mechanism of inhibition.

ARTICLE HISTORY

Received 23 November 2015
Revised 14 February 2016
Accepted 18 February 2016

KEYWORDS

ATM kinase; ataxia telangiectasia; DNA damage response; DNA damage; electron microscopy (EM); PIKK; post-translational modification (PTM)

Introduction

ATM initiates the mammalian DNA-damage response (DDR) through the Mre11/Rad50/Nbs1 (MRN) complex at the damage sites.^{1–4} Specifically, direct interaction with the MRN complex bound to DNA leads to ATM activation, resulting in its conversion of a catalytically inactive homodimer to an active monomeric form⁵ that phosphorylates numerous downstream targets critical for cell-cycle checkpoints, apoptosis and DNA repair.^{4,6–8} Notably, mutations in the ATM gene cause ataxia telangiectasia (A-T), a rare hereditary disorder characterized by progressive neurodegeneration, radiosensitivity, immunodeficiency and cancer predisposition, all of which are hallmarks of deficiencies in the DDR machinery.^{9–11} Knowledge on the structure-function relationship of ATM at the molecular level is paramount to the understanding of its multifaceted role in the maintenance of genome stability.

Monomeric ATM is a large polypeptide of 350 kDa that belongs to the family of PIKKs. The family of PIKKs also includes ataxia-telangiectasia and Rad3-related (ATR), DNA-dependent protein kinase catalytic subunit (DNA-PKcs), as well as mTOR, among others.^{12,13} All members of the PIKK family possess a kinase domain at the C-terminal region of the protein, which shares significant homology with the catalytic domain of phosphatidylinositol 3-kinase (PI3K). Two additional domains of homology are also found within this C-terminal region, including the FRAP, ATM and TRRAP (FAT) domain and the FATC domain that are located N-terminal and C-terminal to the kinase domain, respectively.^{14,15} While the C-terminal region is conserved throughout the PIKK family,

the large N-terminal region exhibits considerable sequence variation and is comprised of repeated units of α helical HEAT repeat motifs.¹⁶ These motifs likely act as scaffolds in mediating protein-protein and protein-DNA interactions,^{17–19} facilitating the interaction of these enzymes with diverse cellular partners and their recruitment to sites of DNA lesions. Indeed, several ATM-interacting proteins have been shown to bind to this region, such as Nbs1 of the MRN complex,^{20,21} ATMIN (ATM Interacting protein)²² and the prostate tumor suppressor NKX3.1.²³ A number of reported subnanometer resolution structures of PIKK enzymes have shed light onto the unique structural aspects of this kinase family. The crystal structure of an N-terminally truncated mTOR in complex with mLST8 at 3.2 Å resolution shows that the kinase domain is clamped on by the FAT domain, and this unique architecture may be a common feature among members of the PIKK family.²⁴ In that structure, the FATC domain is integrated with the kinase domain. The recently determined cryo-electron microscopy (cryo-EM) structure of the mTORC1 (mTOR with subunits Raptor and mLST8) at 5.9 Å resolution reveals that the N-terminal region consists of elongated, α -solenoid helical repeats that are organized into a “horn” and a “bridge.”²⁵ On the other hand, in the crystal structure of the DNA-PKcs, determined to 6.6 Å resolution, the circular arrangement of the HEAT repeats within the N-terminal region gives rise to a ring structure.²⁶ Currently, no high-resolution structures have been reported for intact ATM or any fragments thereof.

Analogous to PI3K enzymes, members of the PIKK family are strongly autoinhibited for their kinase activity in the resting state and only become active upon interactions with their binding

CONTACT Wilson C. Y. Lau  wyclau@hku.hk  School of Biomedical Sciences, Li Ka Shing Faculty of Medicine, The University of Hong Kong, L1-42, Laboratory Block, 21 Sassoon Road, Pokfulam, Hong Kong; Michael S. Y. Huen  huen.michael@hku.hk  School of Biomedical Sciences, Li Ka Shing Faculty of Medicine, The University of Hong Kong, L1-46, Laboratory Block, 21 Sassoon Road, Pokfulam, Hong Kong.

Color versions of one or more of the figures in the article can be found online at www.tandfonline.com/kccy.

© Wilson C. Y. Lau, Yinyin Li, Zhe Liu, Yuanzhu Gao, Qinfen Zhang, and Michael S. Y. Huen. Published with license by Taylor & Francis.

This is an Open Access article distributed under the terms of the Creative Commons Attribution-Non-Commercial License (<http://creativecommons.org/licenses/by-nc/3.0/>), which permits unrestricted non-commercial use, distribution, and reproduction in any medium, provided the original work is properly cited. The moral rights of the named author(s) have been asserted.

partners. To date, limited structural information is available on ATM, despite its fundamental importance in the regulation of the DDR. Herein we report the structure of full-length human ATM in the resting, dimeric state, determined by single-particle EM. Our data advances the current understanding of the molecular architecture of ATM and provides a first glimpse of the structural requirements underlying its inhibitory mechanism.

Results

To carry out structural analysis, we transiently overexpressed human ATM in 293T cells and purified *via* a Flag-tag on its N-terminus under mild conditions that preserve both the monomeric and dimeric forms of the enzyme, as previously described.^{1,2,27} Our one-step purification using anti-Flag affinity resin yielded highly purified enzymes as determined by silver-stained gel (Fig. 1A), albeit the concentration of the preparation was very low (0.02 mg/mL). The inherent difficulty in obtaining large quantities of purified ATM prompted us to carry out negative-stain EM on continuous carbon support. The resulting EM micrographs showed monodisperse particles, but there appeared to be two distinct populations of particles of different sizes (Fig. 1B; Fig. 2A). Following iterative reference-free alignment and classification, we obtained two-dimensional (2D) class averages that clearly revealed the presence of monomeric and dimeric ATM in our preparation, representing about 40% and 60% of the particles, respectively (Fig. 2B and C). It is apparent from the class averages that the dimeric ATM, which has dimensions about twice that of the corresponding monomer, exhibits two-fold symmetry, in agreement with the homodimeric nature of the complex. We followed a multi-reference classification approach to separate the monomeric and dimeric

forms of ATM and calculated a final reconstruction of the ATM in the dimeric state at 26 Å resolution (Fig. 3A; Fig. 4A). Good agreement was observed between the reference-free class averages and the corresponding projections from the map of the dimeric ATM (Fig. 2C). On the other hand, structural heterogeneity and strong preferred particle orientation on the carbon support likely limited our ability to obtain a stable reconstruction of the monomeric ATM, thus precluding further analysis of the three-dimensional (3D) structure.

The dumbbell appearance observed in some of the 2D class averages of monomeric ATM suggested that it adopts an overall bilobed architecture (Fig. 2B). By contrast, the 3D map of dimeric ATM adopts a remarkably different structure that resembles the shape of a butterfly (Fig. 4A). The unambiguous delineation of the subunit and domain boundaries of the EM map permitted segmentation of the density of ATM monomer as well as the disk-like, C-terminal FAT/kinase/FATC region within the monomer (Fig. 4B). In the crystal structure of the N-terminally truncated mTOR, the FAT domain has an appearance of a ring formed by α helical segments and clamps onto the kinase domain.²⁴ Both the kinase and the FAT domains also form similar interaction in the refined electron density map of DNA-PKcs.^{24,26} It has been suggested that these two domains may also assume similar configurations in ATM, as the helical segments of the FAT domain found adjacent to the kinase domain are highly conserved throughout the PIKK family.^{12,26} The kinase domain is also highly conserved in sequence similarity among the family members with an average sequence identity of about 30% (40% identity between ATM and mTOR)¹⁵. We were able to dock this truncated mTOR crystal structure as a rigid body into the segmented density with high fidelity, which provides strong evidence that the

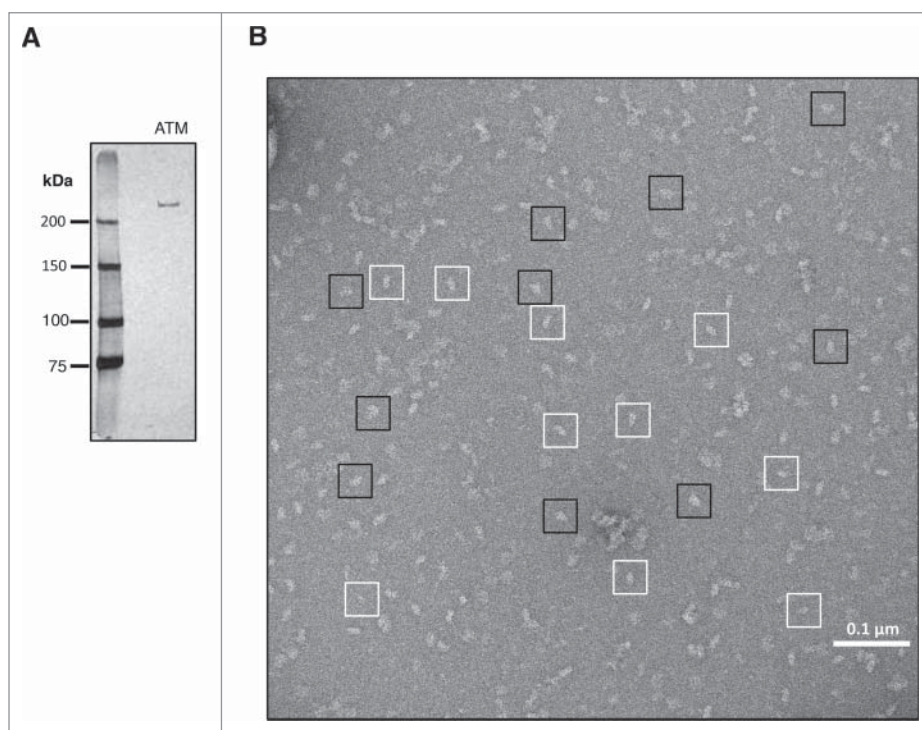


Figure 1. Specimen preparation and EM imaging. (A) Silver-stained SDS-PAGE gel of human ATM purified from 293T cells. (B) Representative negative-stain EM micrograph of purified human ATM. Examples of individual ATM monomers and dimers particles are boxed in white and black, respectively.

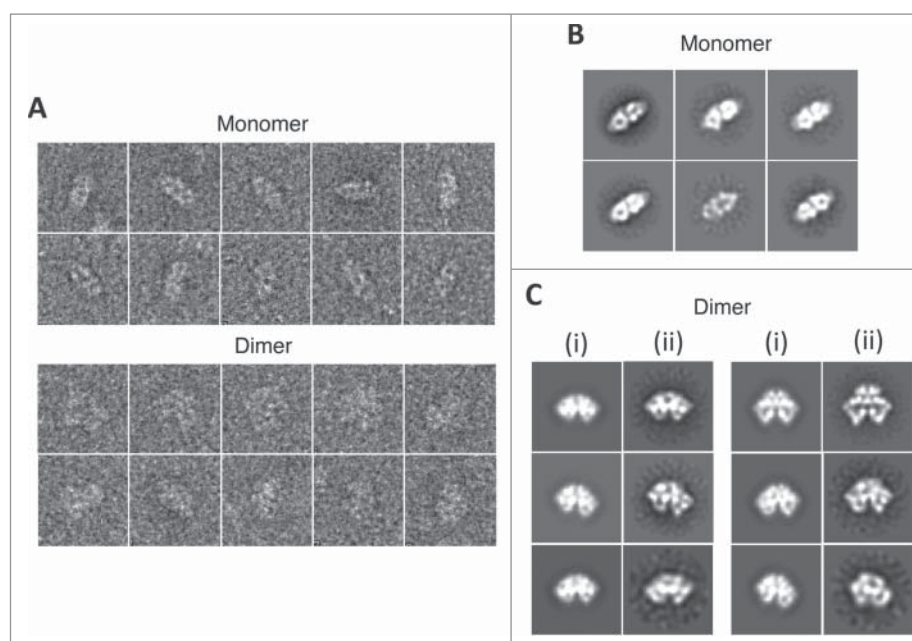


Figure 2. 2D image processing. (A) Examples of individual boxed-out raw particles. (B) Reference-free class averages of ATM monomer. (C) Comparison between representative map projections of ATM dimer (i) and their corresponding reference-free class averages (ii) in the same orientations.

bimodal interaction between these two domains is also congruent with those of mTOR and DNA-PKcs (Fig. 4C). The unoccupied EM density not accounted for by the crystal structure can be attributed to the N-terminal region of ATM, which is organized into a 'head' and a 'tail' domain (Fig. 5). Whereas the C-terminal regions are positioned relatively far apart from each other in the dimeric structure, the tail domains are

juxtaposed around the central two-fold axis of the complex, likely contributing to the interactions of subunits. The N-terminal HEAT repeats have also been implicated in the dimerization of DNA-PKcs.²⁸ For mTOR, dimerization occurs through the interaction between the first HEAT repeat of the N-terminal region with the FAT domain from the opposing subunit of the dimer as seen by cryo-EM.²⁵ The distinct modes of

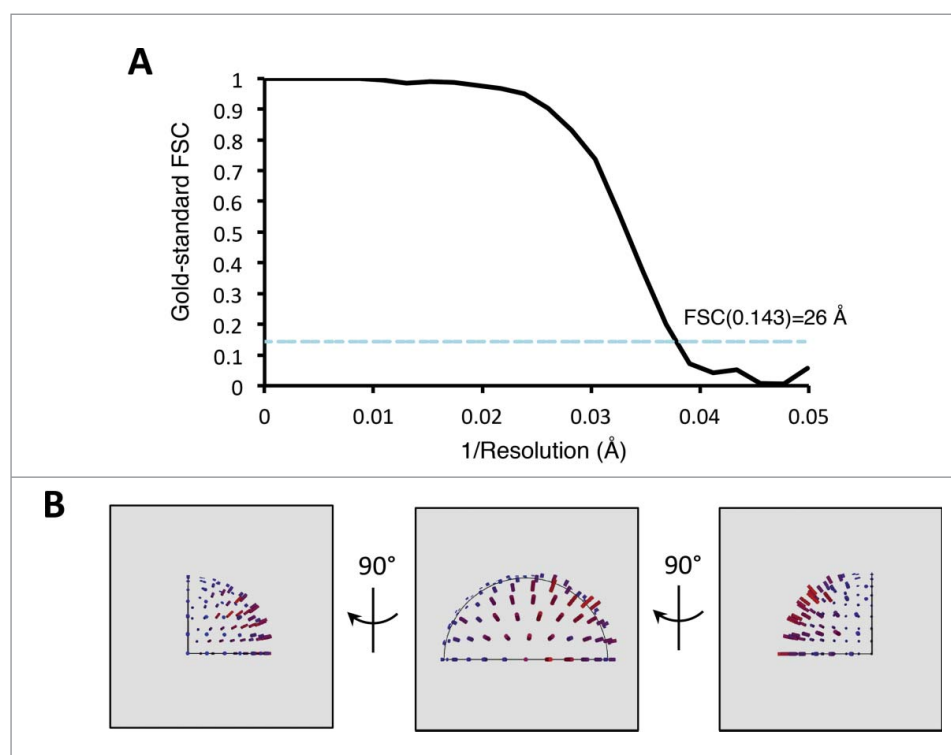


Figure 3. 3D reconstruction. (A) Resolution estimation for the 3D reconstructions by the gold-standard Fourier shell correlation (FSC) plot. (B) Euler angle distribution plots showing the asymmetric unit for the 3D reconstruction. The height of the bar is proportional to the number of particles assigned to that projection. Note that the ATM dimer structure was reconstructed with C2 symmetry imposed.

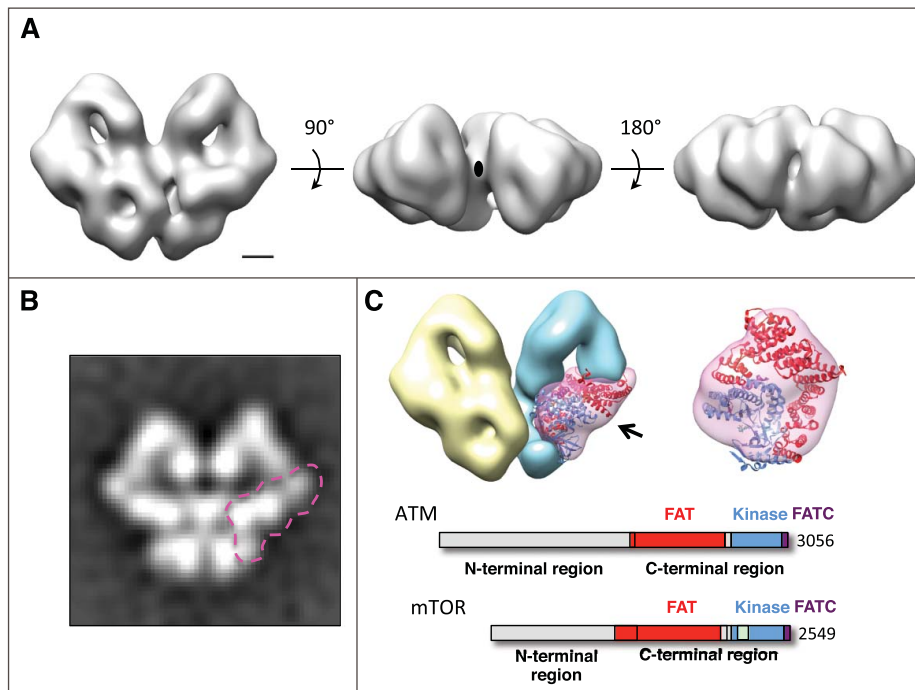


Figure 4. Overall structure of ATM dimer, volume segmentation and rigid-body fitting of atomic model into the EM map revealing the location of the N-terminal and the C-terminal regions. (A) EM map of the dimeric ATM in different views. The 2-fold symmetry axis is indicated with an oval. Scale bar represents 25 Å. (B) Reference-free class average showing the end-on view of the ATM dimer. The C-terminal FAT/kinase/FATC region within one of the monomers is outlined. (C) Left, volume segmentation of the EM map. The two monomers are distinguished by different colors (yellow and blue). The C-terminal FAT/kinase/FATC region on one of the monomers is displayed in semi-transparent pink with the crystal structure of the N-terminally truncated mTOR (PDB ID 4JSV) docked in. Right, blown-up view showing the fit between the mTOR crystal structure and the corresponding map segment. The viewing direction is indicated on the left with an arrow. The domain structures of ATM and mTOR in schematic representation are included. ATM: FAT domain (1966–2566), kinase domain (2614–2960), FATC domain (3025–3056). mTOR: FAT domain (1385–2002), kinase domain (2003–2450), FATC domain (2518–2549). The domains of the crystal structure are colored according to the schematic representation. The region consisting of residues 2021–2118 (FRB domain; light green) is removed from the crystal structure since this insertion region is not conserved in ATM.

interactions mediated through the N-terminal regions of the PIKK family members are not unexpected, as these regions have no apparent sequence similarity among each other.

Discussion

The predominant form of ATM in unstressed cells is homodimeric and catalytically inactive. DNA damage triggers the monomerization and thus the activation of the ATM homodimer through an ill-defined mechanism. In this work, we show that both the N- and the C-terminal regions of each monomer physically associate with that of the other monomer within the dimer, where each monomer likely participates in blocking the activity of the other monomer, leading to an auto-inhibited state. How does the self-association of ATM lead to inhibition of its kinase activity? On the basis of our docking result, the substrate-binding sites are deeply buried in the interior of the complex such that they are physically hindered where access to these sites is highly restricted (Fig. 5). Specifically, the close proximity of the tail domain of the N-terminal region with respect to the active-site cleft in trans results in enclosure of its opening to ~ 10 Å. This architectural element bears a striking resemblance to the recently reported studies showing that access to the active-site cleft of the human mTORC1 complex bound to FK506 binding protein (FKBP)-rapamycin is also restricted by the relative positioning of the FRB domain, FKBP, mLST8 and the RNC domain of Raptor, leading to inhibition of the activity of the complex.²⁵ Therefore,

kinase inhibition by steric hindrance appears to be a common mechanism for both ATM and mTOR.

Autophosphorylation has been suggested to be important for ATM function, and ATM activation is always accompanied by autophosphorylation at serine 1981 *in vivo*. Upon monomerization, S1981 phosphorylation could play a role in preventing the re-association of the ATM monomers back to dimers.²⁰ Based on *in vitro* biochemical data, Bakkenist and Kastan proposed that the kinase domain binds to a region in the FAT domain surrounding S1981 in the dimer.⁵ The present front-to-front arrangement of the monomers within the dimeric complex does not favorably support this model because the FAT domains are situated away from the interface of the monomers (Fig. 5; Fig. 6). Nonetheless, we do not formally exclude this model owing to low resolution of the EM map. Notably, our current model is consistent with ATM autophosphorylation being dispensable for its activation in mice, as shown in previous studies.^{29,30}

The MRN complex has been identified to play an indispensable role in the localization and activation of ATM. Not only it promotes localization of ATM to the sites of DSBs through engagement to both DSBs and ATM, it also facilitates its dimer-to-monomer conversion process through direct binding as well as presenting DSB ends to ATM, simultaneously. The last 20 amino acid residues at the C-terminus of the Nbs1 component of the MRN complex has been shown to contact ATM and is essential for its activation.^{20,21} In yeast, this short stretch of residues interacts with a HEAT repeat segment in the N-

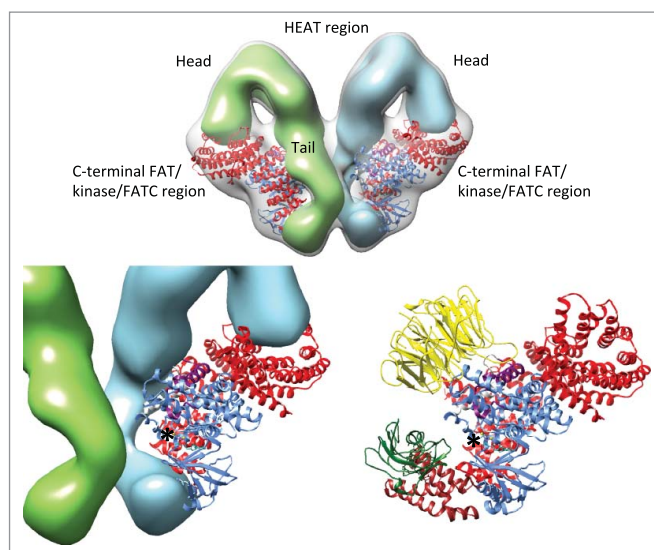


Figure 5. Intersubunit interaction and proposed mechanism of kinase activity inhibition. The N-terminal regions comprising of HEAT repeats are represented in solid surface. The head and the tail domains of the N-terminal region are labeled. The domains of the mTOR crystal structure are colored according to the schematic representation in Fig. 4C. The EM map is represented in semi-transparent gray surface. The kinase activity center is indicated with an asterisk. Bottom left, the distance between the tail domain and the active site is 70 Å. Bottom right, similar restriction of the active-site cleft due to the presence of mLST8 (yellow), the FRB insertion (brown) and FKBP-rapamycin in mTOR. The RNC domain of Raptor is omitted for clarity.

terminal region of Tel, an ortholog of ATM.³¹ The Mre11-Rad50 component also binds ATM, although the corresponding interaction surface on ATM has not been mapped.¹ According to our structure, it is conceivable that the MRN complex, which itself is also a dimer, recognizes the large concave surface in the ATM dimer formed by the head domains of the N-terminal regions *via* multiple contacts in order to elicit the dimer dissociation reaction. This vertex region of the dimer may also contain putative DNA-binding sites formed by HEAT repeats. A domain comprising of HEAT repeats has also been ascribed to the putative DNA-binding site in the N-terminal

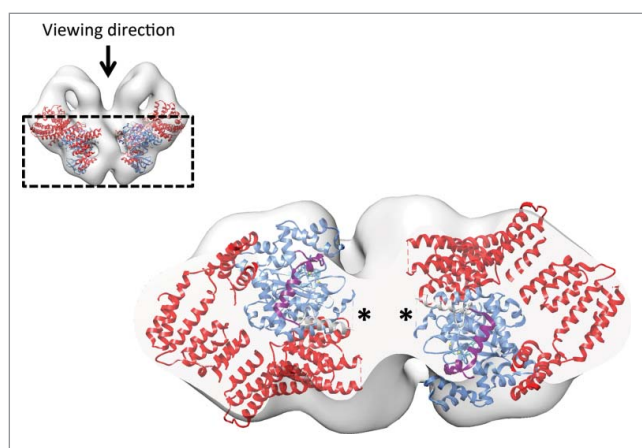


Figure 6. Localization of the C2991 residue in ATM necessary for activation via the oxidative mechanism. The top portion of the map is removed for clarity. The locations of the variable loop consisting of residues 2437–2491, which is disordered in the crystal structure, are indicated with asterisks. This loop region contains the critical residue C2991 in the corresponding ATM structure that is essential for its oxidation activation. The domains of the mTOR crystal structure are colored according to the schematic representation in Fig. 4C.

region of DNA-PKcs.²⁶ Support for the notion that HEAT repeats can mediate protein-DNA interactions come from the previous studies of the DNA glycosylase AlkD and condensins.^{18,19}

Recently, Paull and colleagues have elucidated an MRN/DNA-independent mechanism of ATM activation.^{32,33} This alternative activation mechanism is induced by oxidative stress. *In vitro*, exposure of ATM to hydrogen peroxide resulted in the formation of a disulfide-cross-linked dimer that is also catalytically active. A cysteine residue 2991 within the FATC domain was found to be absolutely necessary for this oxidation-dependent activation. Mutation of this residue did not affect the MRN/DNA-dependent activation, however, suggesting the presence of two distinct mechanisms of activation for ATM. Even though this critical residue C2991 is found in a loop region that is disordered in the mTOR crystal structure,^{12,24} fitting of the crystal structure into the EM map revealed that these residues would be localized to the central region of the dimer (Fig. 6). This observation is consistent with a disulfide bond being able to form under oxidizing conditions only if these cysteines are in close proximity to each other in the dimer. We posit that the formation of this disulfide could lead to reorganization of the monomer-monomer interface, leading to exposure of the catalytic and substrate-binding sites.

We noted that our structure of monomeric ATM obtained from segmentation of the EM map is markedly different compared to the published structure of the same enzyme.³⁴ While such a discrepancy may be explained by gross conformational changes associated with the dimer-to-monomer conversion, the inconsistency between our obtained class averages of the ATM monomer and the expected 2D projections of the published structure makes this assumption highly unlikely and awaits further studies. In conclusion, the structure reported here unravels a central mechanism of regulation of ATM activity and pave the way for higher resolution cryo-EM studies on ATM and ATM-containing complexes.

Materials and methods

Protein preparation

The pcDNA-FLAG-His-ATM wt expression construct encoding full-length human ATM. Protein purification was carried out as described previously with slight modifications.²⁷ Cells were lysed by homogenization on ice in buffer containing 25 mM Tris pH 8.0, 250 mM NaCl, 20 mM MgCl₂, 0.5 mM phenylmethylsulfonyl fluoride (PMSF), 1 mM Tris(2-carboxyethyl)phosphine hydrochloride (TCEP), 20% glycerol. After centrifugation at 10000g for 15 min at 4°C, the supernatant was collected and incubated with anti-Flag M2 affinity gel (Biotool) for 1 hr at 4°C. The resin was washed twice with the same buffer followed by twice with buffer A (25 mM Tris pH 8.0, 100 mM NaCl, 1 mM TCEP, 10% glycerol). Proteins were eluted from the resin with 100 µg/mL Flag peptide (Sigma) in buffer A. To remove the Flag peptide, eluted proteins were finally dialyzed in buffer A using a Slide-A-Lyzer MINI Dialysis Device (ThermoFisher Scientific). TCEP was included in all purification steps to avoid spontaneous oxidation of ATM. The purity of

the eluted fractions was estimated to be >95% by silver staining. A total of 5 µg protein could be obtained from 0.8 – 1L of media. Purified ATM was used immediately for EM analysis.

Electron microscopy specimen preparation and data acquisition

Samples were stained with 2% (w/v) uranyl acetate following an established protocol using freshly glow-discharged, continuous carbon coated copper grids (Ted Pella). Images of ATM were acquired on a JEOL JEM2010 electron microscope operated at 200 kV using a Gatan Ultrascan 4k x 4k CCD camera at a nominal magnification of 50kx, corresponding to a calibrated pixel size of 2.14 Å at the specimen level. The electron exposure was adjusted to ~20–30 electrons/Å.² The data was recorded with defocuses ranged between –1 and –4 µm.

Image processing

Image processing steps were carried out in EMAN 2.1³⁵ and RELION 1.4.³⁶ A total of 13833 particles were selected either manually or semi-automatically and the contrast transfer function (CTF) parameters were determined from windowed particle images in EMAN. Subsequent iterative reference-free 2D image classification in RELION using phase-flipped particles without further CTF correction revealed the presence of two distinct populations of particles within the sample, which correspond to the monomeric and the dimeric forms of ATM. Initial model generation was performed using two independent approaches. In the first approach, a subset of these class averages was selected as inputs for ‘e2initialmodel.py’ within EMAN to obtain starting models of the monomer and dimer of ATM, followed by multi-reference 3D classification using ‘e2refinmulti.py’ to separate the dataset into two distinct particle populations and to improve the starting models. In the second approach, the particles were directly extracted from the class averages to generate two distinct particle population, followed by the *ab initio* reconstruction algorithm PRIME in the SIMPLE 2.0 software package to produce the starting models.³⁷ Using the independent subsets of data either extracted from 2D or 3D classification as described above, final iterative 3D refinements with full CTF correction against the starting models were carried out by the gold-standard procedure in EMAN. Only spatial frequencies up to 1/35Å were used during the refinement to avoid noise fitting, where Fourier ring correlation was used as the similarity comparator. For dimeric ATM, since clear two-fold symmetry was apparent in the reference-free class averages and the starting models, hence, subsequent refinement was carried out with C2 symmetry imposed. Both approaches produced maps that are nearly identical for the dimeric data set but not for the monomeric dataset, and therefore the monomeric data set was omitted for further analysis. The resolution of the final 3D reconstruction of the ATM dimer was estimated to be 26 Å by the Fourier shell correlation (FSC) 0.143 cut-off.³⁸

Map interpretation, visualization and validation

Semi-automatic volume segmentation using the watershed algorithm, rigid-body docking, visualization and rendering were performed using UCSF Chimera.³⁹ Segmentation and molecular docking was carried out with the Segger routine⁴⁰ and the ‘Fit-in-map’ option in Chimera, respectively. The comparison between the map projections and the corresponding reference-free class averages highlighted the self-consistency of our final 3D reconstruction. The excellent agreement between the fitted crystal structure and the map segment provided support to the validity of our map. The map was further validated by the tilt-pair test with pairs of images of the same field recorded at 0 and +10°.

Abbreviations

ATM	ataxia-telangiectasia mutated
EM	electron microscopy
Mtor	mammalian target of rapamycin
PIKK	phosphatidylinositol 3-kinase-related protein kinase
DDR	DNA-damage response
MRN	Mre11/Rad50/Nbs1
A-T	ataxia telangiectasia
ATR	ataxia-telangiectasia and Rad3-related
DNA-PKcs	DNA-dependent protein kinase catalytic subunit
PI3K	phosphatidylinositol 3-kinase
FAT	FRAP, ATM and TRRAP
ATMIN	ATM INteracting protein
cryo-EM	cryo-electron microscopy
3D	Three-dimensional
2D	Two-dimensional
PMSF	phenylmethylsulfonyl fluoride
TCEP	Tris(2-carboxyethyl)phosphine hydrochloride
FSC	Fourier shell correlation

Disclosure of potential conflicts of interest

No potential conflicts of interest were disclosed.

Acknowledgments

We gratefully acknowledge J. Rubinstein (University of Toronto) for providing access to the Sickkids High Performance Facility for calculations with RELION. The mammalian expression vector pcDNA-FLAG-His-ATM wt was a gift from M. Kastan (Duke University Cancer Institute). We thank the staff at the Electron Microscope Unit at The University of Hong Kong for access to facilities and invaluable help.

Funding

This work was supported by fund from Research Grants Council Hong Kong – Early Career Scheme 2012 (Project Number: 786512). W.C.Y.L. was supported by an AXA Research Fund fellowship.

Author contributions

MSYH and WCYL initiated the project. WCYL designed and carried out all the experiments, including protein purification, data acquisition and image processing. YL, ZL and YG provided technical assistance with performing EM imaging. YG and QZ contributed EM tools and provided

access to EM facilities. WCYL interpreted the data and wrote the manuscript with contribution from MSYH.

Accession numbers

The EM maps of ATM have been deposited in the EMDB under accession numbers 6501. The atomic coordinates for the fitted crystal structure have been deposited in the PDB under accession numbers 3JBZ.

References

- [1] Lee JH, Paull TT. Direct activation of the ATM protein kinase by the Mre11/Rad50/Nbs1 complex. *Science* 2004; 304:93-6; PMID:15064416; <http://dx.doi.org/10.1126/science.1091496>
- [2] Lee JH, Paull TT. ATM activation by DNA double-strand breaks through the Mre11-Rad50-Nbs1 complex. *Science* 2005; 308:551-4; PMID:15790808; <http://dx.doi.org/10.1126/science.1108297>
- [3] Uziel T, Lerenthal Y, Moyal L, Andegeko Y, Mittelman L, Shiloh Y. Requirement of the MRN complex for ATM activation by DNA damage. *EMBO J* 2003; 22:5612-21; PMID:14532133; <http://dx.doi.org/10.1093/emboj/cdg541>
- [4] Shiloh Y, Ziv Y. The ATM protein kinase: regulating the cellular response to genotoxic stress, and more. *Nat Rev Mol Cell Biol* 2013; 14:197-210; <http://dx.doi.org/10.1038/nrm3546>
- [5] Bakkenist CJ, Kastan MB. DNA damage activates ATM through intermolecular autophosphorylation and dimer dissociation. *Nature* 2003; 421:499-506; PMID:12556884; <http://dx.doi.org/10.1038/nature01368>
- [6] Berkovich E, Monnat RJ, Jr, Kastan MB. Roles of ATM and NBS1 in chromatin structure modulation and DNA double-strand break repair. *Nat Cell Biol* 2007; 9:683-90; PMID:17486112; <http://dx.doi.org/10.1038/ncb1599>
- [7] Bensimon A, Schmidt A, Ziv Y, Elkou R, Wang SY, Chen DJ, Aebersold R, Shiloh Y. ATM-dependent and -independent dynamics of the nuclear phosphoproteome after DNA damage. *Sci Signal* 2010; 3:rs3; PMID:21139141
- [8] Matsuoka S, Ballif BA, Smogorzewska A, McDonald ER, 3rd, Hurov KE, Luo J, Bakalarski CE, Zhao Z, Solimini N, Lerenthal Y, et al. ATM and ATR substrate analysis reveals extensive protein networks responsive to DNA damage. *Science* 2007; 316:1160-6; PMID:17525332; <http://dx.doi.org/10.1126/science.1140321>
- [9] Alvarez-Quilon A, Serrano-Benitez A, Lieberman JA, Quintero C, Sanchez-Gutierrez D, Escudero LM, Cortes-Ledesma F. ATM specifically mediates repair of double-strand breaks with blocked DNA ends. *Nat Commun* 2014; 5:3347; PMID:24572510; <http://dx.doi.org/10.1038/ncomms4347>
- [10] McKinnon PJ. ATM and ataxia telangiectasia. *EMBO Reports* 2004; 5:772-6; PMID:15289825; <http://dx.doi.org/10.1038/sj.embor.7400210>
- [11] Jackson SP, Bartek J. The DNA-damage response in human biology and disease. *Nature* 2009; 461:1071-8; PMID:19847258; <http://dx.doi.org/10.1038/nature08467>
- [12] Paull TT. Mechanisms of ATM Activation. *Ann Rev Biochem* 2015; 84:711-38; PMID:25580527; <http://dx.doi.org/10.1146/annurev-biochem-060614-034335>
- [13] Lovejoy CA, Cortez D. Common mechanisms of PIKK regulation. *DNA Repair* 2009; 8:1004-8; PMID:19464237; <http://dx.doi.org/10.1016/j.dnarep.2009.04.006>
- [14] Lempiainen H, Halazonetis TD. Emerging common themes in regulation of PIKKs and PI3Ks. *EMBO J* 2009; 28:3067-73; PMID:19779456; <http://dx.doi.org/10.1038/emboj.2009.281>
- [15] Bosotti R, Isacchi A, Sonhammer EL. FAT: a novel domain in PIK-related kinases. *Trends Biochem Sci* 2000; 25:225-7; PMID:10782091; [http://dx.doi.org/10.1016/S0968-0004\(00\)01563-2](http://dx.doi.org/10.1016/S0968-0004(00)01563-2)
- [16] Perry J, Kleckner N. The ATRs, ATMs, and TORs are giant HEAT repeat proteins. *Cell* 2003; 112:151-5; PMID:12553904; [http://dx.doi.org/10.1016/S0092-8674\(03\)00033-3](http://dx.doi.org/10.1016/S0092-8674(03)00033-3)
- [17] Andrade MA, Petosa C, O'Donoghue SI, Muller CW, Bork P. Comparison of ARM and HEAT protein repeats. *J Mol Biol* 2001; 309:1-18; PMID:11491282; <http://dx.doi.org/10.1006/jmbi.2001.4624>
- [18] Piazza I, Rutkowska A, Ori A, Walczak M, Metz J, Pelechano V, Beck M, Haering CH. Association of condensin with chromosomes depends on DNA binding by its HEAT-repeat subunits. *Nat Structural Mol Biol* 2014; 21:560-8; <http://dx.doi.org/10.1038/nsmb.2831>
- [19] Rubinson EH, Gowda AS, Spratt TE, Gold B, Eichman BF. An unprecedented nucleic acid capture mechanism for excision of DNA damage. *Nature* 2010; 468:406-11; PMID:20927102; <http://dx.doi.org/10.1038/nature09428>
- [20] Dupre A, Boyer-Chatenet L, Gautier J. Two-step activation of ATM by DNA and the Mre11-Rad50-Nbs1 complex. *Nat Structural Mol Biol* 2006; 13:451-7; <http://dx.doi.org/10.1038/nsmb1090>
- [21] Falck J, Coates J, Jackson SP. Conserved modes of recruitment of ATM, ATR and DNA-PKcs to sites of DNA damage. *Nature* 2005; 434:605-11; PMID:15758953; <http://dx.doi.org/10.1038/nature03442>
- [22] Kanu N, Behrens A. ATMIN defines an NBS1-independent pathway of ATM signalling. *EMBO J* 2007; 26:2933-41; PMID:17525732; <http://dx.doi.org/10.1038/sj.emboj.7601733>
- [23] Bowen C, Ju JH, Lee JH, Paull TT, Gelmann EP. Functional activation of ATM by the prostate cancer suppressor NKX3.1. *Cell Reports* 2013; 4:516-29; PMID:23890999; <http://dx.doi.org/10.1016/j.celrep.2013.06.039>
- [24] Yang H, Rudge DG, Koos JD, Vaidialingam B, Yang HJ, Pavletich NP. mTOR kinase structure, mechanism and regulation. *Nature* 2013; 497:217-23; PMID:23636326; <http://dx.doi.org/10.1038/nature12122>
- [25] Aylett CH, Sauer E, Imseng S, Boehringer D, Hall MN, Ban N, Maier T. Architecture of human mTOR complex 1. *Science* 2016; 351:48-52; PMID:26678875; <http://dx.doi.org/> <http://dx.doi.org/10.1126/science.aaa3870>
- [26] Sibanda BL, Chirgadze DY, Blundell TL. Crystal structure of DNA-PKcs reveals a large open-ring cradle comprised of HEAT repeats. *Nature* 2010; 463:118-21; PMID:20023628; <http://dx.doi.org/10.1038/nature08648>
- [27] Lee JH, Paull TT. Purification and biochemical characterization of ataxia-telangiectasia mutated and Mre11/Rad50/Nbs1. *Methods Enzymol* 2006; 408:529-39; [http://dx.doi.org/10.1016/S0076-6879\(06\)08033-5](http://dx.doi.org/10.1016/S0076-6879(06)08033-5)
- [28] Morris EP, Rivera-Calzada A, da Fonseca PC, Llorca O, Pearl LH, Spagnolo L. Evidence for a remodelling of DNA-PK upon autophosphorylation from electron microscopy studies. *Nucleic Acids Res* 2011; 39:5757-67; PMID:21450809; <http://dx.doi.org/10.1093/nar/gkr146>
- [29] Daniel JA, Pellegrini M, Lee JH, Paull TT, Feigenbaum L, Nussenzweig A. Multiple autophosphorylation sites are dispensable for murine ATM activation in vivo. *J Cell Biol* 2008; 183:777-83; PMID:19047460; <http://dx.doi.org/10.1083/jcb.200805154>
- [30] Pellegrini M, Celeste A, Difilippantonio S, Guo R, Wang W, Feigenbaum L, Nussenzweig A. Autophosphorylation at serine 1987 is dispensable for murine Atm activation in vivo. *Nature* 2006; 443:222-5; PMID:16906133; <http://dx.doi.org/10.1038/nature05112>
- [31] You Z, Chahwan C, Bailis J, Hunter T, Russell P. ATM activation and its recruitment to damaged DNA require binding to the C terminus of Nbs1. *Mol Cell Biol* 2005; 25:5363-79; PMID:15964794; <http://dx.doi.org/10.1128/MCB.25.13.5363-5379.2005>
- [32] Guo Z, Deshpande R, Paull TT. ATM activation in the presence of oxidative stress. *Cell Cycle* 2010; 9:4805-11; PMID:21150274; <http://dx.doi.org/10.4161/cc.9.24.14323>
- [33] Guo Z, Kozlov S, Lavin MF, Person MD, Paull TT. ATM activation by oxidative stress. *Science* 2010; 330:517-21; PMID:20966255; <http://dx.doi.org/10.1126/science.1192912>
- [34] Llorca O, Rivera-Calzada A, Grantham J, Willison KR. Electron microscopy and 3D reconstructions reveal that human ATM kinase uses an arm-like domain to clamp around double-stranded DNA. *Oncogene* 2003; 22:3867-74; PMID:12813460; <http://dx.doi.org/10.1038/sj.onc.1206649>

- [35] Tang G, Peng L, Baldwin PR, Mann DS, Jiang W, Rees I, Ludtke SJ. EMAN2: an extensible image processing suite for electron microscopy. *J Structural Biol* 2007; 157:38-46; <http://dx.doi.org/10.1016/j.jsb.2006.05.009>
- [36] Scheres SH. RELION: implementation of a Bayesian approach to cryo-EM structure determination. *J Structural Biol* 2012; 180:519-30; <http://dx.doi.org/10.1016/j.jsb.2012.09.006>
- [37] Elmlund D, Elmlund H. SIMPLE: Software for ab initio reconstruction of heterogeneous single-particles. *J Structural Biol* 2012; 180:420-7; <http://dx.doi.org/10.1016/j.jsb.2012.07.010>
- [38] Rosenthal PB, Henderson R. Optimal determination of particle orientation, absolute hand, and contrast loss in single-particle electron cryomicroscopy. *J Mol Biol* 2003; 333:721-45; PMID:14568533; <http://dx.doi.org/10.1016/j.jmb.2003.07.013>
- [39] Pettersen EF, Goddard TD, Huang CC, Couch GS, Greenblatt DM, Meng EC, Ferrin TE. UCSF Chimera—a visualization system for exploratory research and analysis. *J Computational Chem* 2004; 25:1605-12; <http://dx.doi.org/10.1002/jcc.20084>
- [40] Pintilie G, Chiu W. Comparison of Segger and other methods for segmentation and rigid-body docking of molecular components in cryo-EM density maps. *Biopolymers* 2012; 97:742-60; PMID:22696409; <http://dx.doi.org/10.1002/bip.22074>